Experimental Investigation Studying Effect of Width and Pitch of Quadcopter Propeller Blade on Resultant Thrust

Ananya Iyer

Abstract

Multirotor platforms used in the field of unmanned aerial vehicles (UAV) for aerial cinematography often face a lot of flight stability problems due to the aerodynamic forces produced by the propeller geometry. The 6035 propeller blades are popular with beginner drones but slight differences in blade size can heavily alter the thrust and subsequent handling of the vehicle. The purpose of this study is to systematically investigate the effect of changing blade width and blade pitch of a quadcopter propeller blade on the static thrust generated by the propeller, and thus the effect on the stability of aerial photography down stream of the propeller. To achieve an affordable and sustainable prototyping model, the multiple prototype variants of the geometric design were CAD designed and 3D printed, based on a baseline 6035 control propeller. Four different configurations were tested: a standard 3D printed 6035 blade, an increased pitch variant (6045 profile), a width-extended 6035 blade, and a combined hybrid variant with increased pitch and increased chord width. Results indicated that the 3D-printed version and the commercially available control blade were identical, as both generated 39.02 grams of thrust at a low motor speed (1050 μs). Modifying blade shape individually increased thrust. Increasing blade pitch to 6045 resulted in 48.87 grams of thrust. Further increasing thrust to 58.04 grams was achieved by widening the blade. The hybrid blade was the most effective, also increasing thrust, to 73.17 grams, nearly 100% of the original thrust.However, the data pointed out the limits of increasing blade size. Increasing aerodynamic profile and weight of the hybrid blade increased drag, and led to connection glitches in the data logs and excessive thermal stress on the electronic speed controller (ESC). Therefore, wider blades are good for generating the thrust necessary to stabilize a camera drone, but the combination of widening the blades and increasing the pitch also applies the thrust to the limits of the ESP and increases the risk of burning the system out. These results provide a predictive framework for propeller modifications to improve stability and prevent damaging power overloads during filming missions. They also connect the structural additive manufacturing parameters with real UAV flight dynamics.

Introduction

In recent years, interest in UAVs has increased in both academia and industry. This is the result of UAVs being able to be deployed rapidly in a number of different areas, such as Defense infrastructure, commercial logistics, and even mapping. The fast growth of high-definition aerial cinematography has further popularized the use of micro-multi-rotor UAVs in residential and commercial filming requirements. While small UAVs are being ameliorized more and more, they also have common problems with flight stabilization. During filming operations that take place at low altitudes, small disturbances in the atmosphere can cause a significant negative effect on the stabilization of the filmed object and can cause jitters. This can be even more problematic if the stabilization jitters are in a frequency that tracking software can't compensate for. Consumer filming support platforms heavily rely on rapid responses of thrust adjustments to control the position of the craft. This has led to a large focus in the engineering of micro-multi-rotors UAVs that is their optimization.

A considerable amount of research has been dedicated to the basic aerodynamic variables of small-scale rotors, which provides insight into their dynamics. Basic geometric variables such as blade angle, chord width, and rotor solidity are said to impact rotors' thrust most significantly. *Langa (2025)* studied the relationships and found that basic power and aerodynamic characteristics of rotors are most significantly influenced by the pitch and diameter of the rotors, which are the most feasible options for researchers in this field to change [1]. Other researchers, however, may need to account for blade surface and flow intricacies. *Susi et al. (2025)* studied the low Reynolds number regime efficiency of small-scale rotors and characterized slipstream velocities to reveal locations of transition from liquid and gas flow and from laminar to turbulent in the fields of flow around and within rotors [2]. In light of the above results, there is a trade-off between large scale design variables and local flow variables.

More recent studies have heavily emphasized the analysis of next generation geometric configurations as an alternative way to address traditional performance challenges. For example, *Rao Ganji et al. (2024)*, worked with advanced computational fluid modeling techniques, showed that closed loop, toroidal propeller geometry, using tip vortex suppression, facilitated improvements on both thrust and fluid performance profiles, while providing significantly better thrust [3]. In a different study, *Gabriel and Simion (2023)* executed rigorous comparative testing of both standard and toroidal forms, while observing their rigidity and the levels of noise [4]. With the complexity of advanced shapes, the benefits of noise reduction and maximization of lift come at the cost of an increase in the challenges of manufacturing. These complications often force engineers to consider sophisticated structures. In this context, *Gowtham (2024)* examined some configurations including ducting and shrouding, to show that the use of structurally rigid shrouding can produce thrust improving, localized suction gradients without blade changes [5].

While costs and infrastructure place limitations on physical aerodynamic testing, computational simulation modeling is more relied on to estimate dynamics of the powertrain. *Eraslan et al. (2020)* conducted an extensive literature review of thrust and power coefficient equations and established a baseline for rotor modeling using math [6]. Besides that, *Vizeu (2023)* closed the gap that existed between low-fidelity Blade Element Theory (BET) math techniques and high-fidelity CFD (Computational Fluid Dynamics) techniques and developed a framework for the assessment of simulated fluid dynamics against real-world measurements [7]. To complement these techniques, physical testing is required to validate the models. *Faishal et al. (2025)* provided an example of the reliability of static ground testing, showing that physical thrust data is highly aligned to math when testing boundary conditions are highly controlled [8].

Even though a variety of computational models can be used, pure simulations usually do not represent the limitations of the materials that are encountered during the actual manufacturing process. This is seen when considering the effect of the number of blades compared to the localized surface area. *Dayhoum et al. (2024)* studied the effect of multi-blade configurations and described the relationship in which an increase in the number of blades changes the hub assembly's configuration which in turn increases the total drag [9]. This effect introduces multiple electromechanical design challenges to the system during operation. *Krmela et al. (2021)* described these trade-offs in the case of drone propellers and stated that the propellers must be of a highly strong material to prevent failure but must also be lightweight to prevent a loss of performance due to deformation of the propellers [10]. *Bağçe (2015)* similarly highlighted that structural mass shifts can massively alter the torque demands imposed on the motor, directly dictating the mechanical power requirements of the overall powertrain system [11].

Existing research focuses mainly on sophisticated forms of geometry like toroidal loops, or on changes in the absolute number of blades. However, published research focuses on a general lack of studies that consider the local scaling of basic blade chord width in relation to blade pitch, especially among readily available consumer platforms. There is little consideration to how these structural changes behave when implemented through low-cost additive manufacturing such as 3D Printing.

This research aims to fill this gap by providing an empirical study that examines how changes made to the width and pitch of an amazon 6035 quadcopter propeller changes thrust generation which thus affects the stability of cinematography. A custom, open-source 3D printed static testing apparatus was utilized to test four propeller blade designs: a standard 3D printed 6035 control propeller, an increased pitch 6035 propeller, an extended chord 6035 propeller, and a propeller integrating both a pitch and chord increase. A limited commercial 3D printed control propeller was compared to all tested designs. Within this framework, this study delineates the thrust generation boundaries and the electromechanical and thermal limits for 3D printed propulsion systems used in commercially available drones.

Methodology: Hardware

1. *Circuit Design*

The electronic setup was built around an Arduino Uno microcontroller, a widely used and proven hardware that controls the hardware timers and the analog-to-digital sensor inputs. The circuit was divided into two electrical paths, one supplying power to the brushless motor (high current) and the other supplying power to the sensor to measure the very small variations in force (low voltage).

A high KV brushless DC motor was connected to an Electronic Speed Controller (ESC) for the motor side of the circuit. The ESC serves as an electronic switch to push heavy current into the motor coils based on commands from the microcontroller. An external 11.1 V Lithium Polymer (LiPo) battery pack was used to power the ESC. The battery was a high discharge type that needed to maintain the voltage received to the motor and avoid voltage drop, when the motor was asked to rotate the larger, higher drag prototype blades. The signal and ground wires of the ESC were wired straight to Digital Pin 9 of the arduino, which was programmed to send out pulses of varying width (Pulse Width Modulation, or PWM) to control the throttle speed.

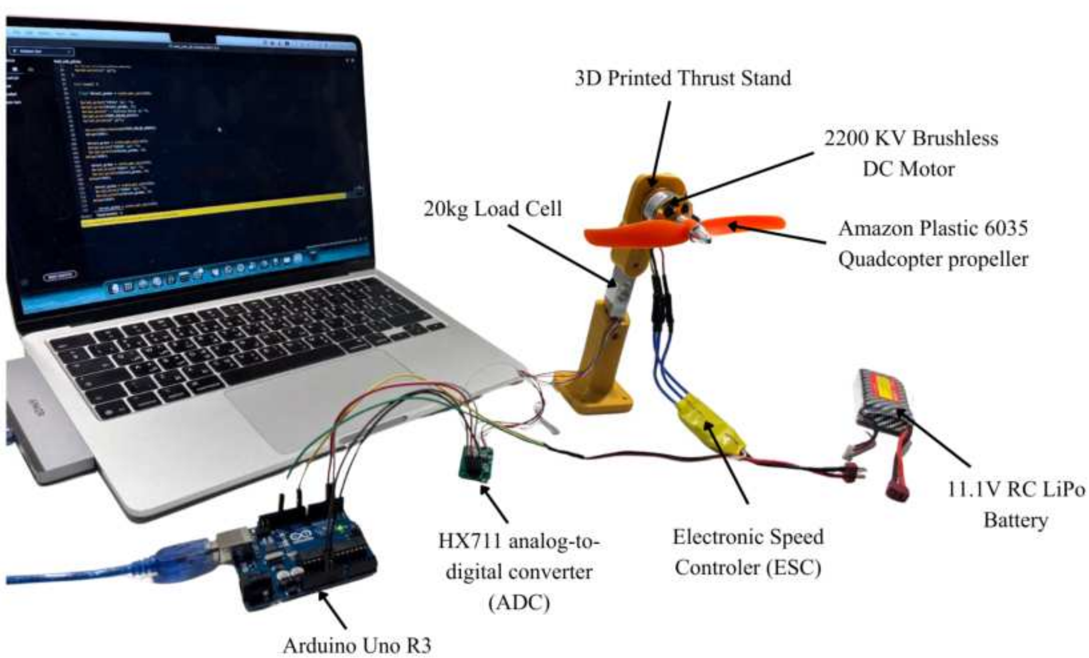

Figure 1: Testing Setup with labelled annotations of equipment

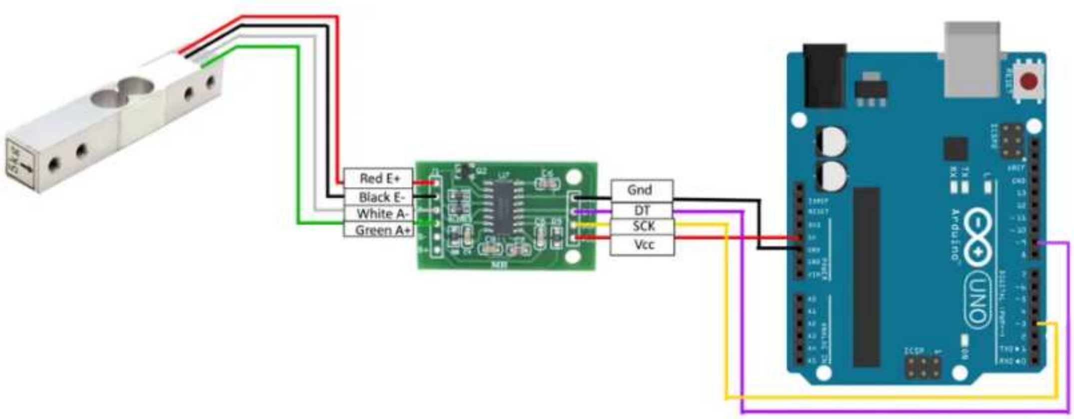

Figure 2: Circuit diagram of load cell to HX711 ADC to Arduino Uno Board

Furthermore, a strain-gauge load cell was used, and was put into the base of the thrust stand framework for the measurement side of the circuit. The propeller rotated and dragged the pivoting arm along causing the load cell sensor to be compressed. This physical pressure distorted the internal strain gauges inside the cell, causing a slight change in electrical resistance, and sending out a small analog voltage signal (micro-volt). This analog voltage difference is too tiny for the analog inputs on the Arduino to accurately measure it with the built-in 10-bit analog-to-digital conversion, so an HX711 analog voltage amplifier and instrumentation module was added into the circuit. This small signal was amplified by the HX711 and was converted into a very accurate 24-bit digital value. The serial data line (DT) and serial clock line (SCK) of the HX711 were connected directly to the digital pins of the arduino and the arduino was connected to a serial port.The serial data line (DT) and the serial clock line (SCK) of the HX711 were connected to the digital pins of the arduino, which was connected to a serial port, so the arduino could read a clean, constant stream of weight values over a serial connection.

2. ***3D-Printed Thrust Stand Manufacturing***

The test rig structure was completely 3D printed from an open-source geometry available on the Instructables project platform called "Brushless Motor Thrust Stand" [13]. It was much easier and more practical to decide to 3D print this piece than to try and cut and drill factory metal or wood plates. The use of a 3D-printer allowed the structural mounting faces to be designed to fit the exact bolt holes of the desired brushless motor and the threaded holes of the load cell sensor perfectly. This customization ensured the build was very close together and also ruled out any unwanted mechanical movement that would destroy the force readings.

The 3D printed stand proved to be absolutely flawless during testing and was able to withstand significant mechanical load. The frame was stiff enough to dampen out high frequency vibrations generated by the high speed brushless motor which made the signal readings from the sensor fairly stable. This stand had a smooth pivot point which translated the forward and horizontal force from the propeller into a clear vertical and downward force on the center of the load cell sensor. Further, the stand was open, so that there were no large flat areas immediately behind the spinning blades. This enabled the air which sucked the propeller to blow directly through the rig in a clean manner and not have artificial ground effect or recirculating air currents to artificially add thrust numbers to the data logs. View Figure 2 for reference.

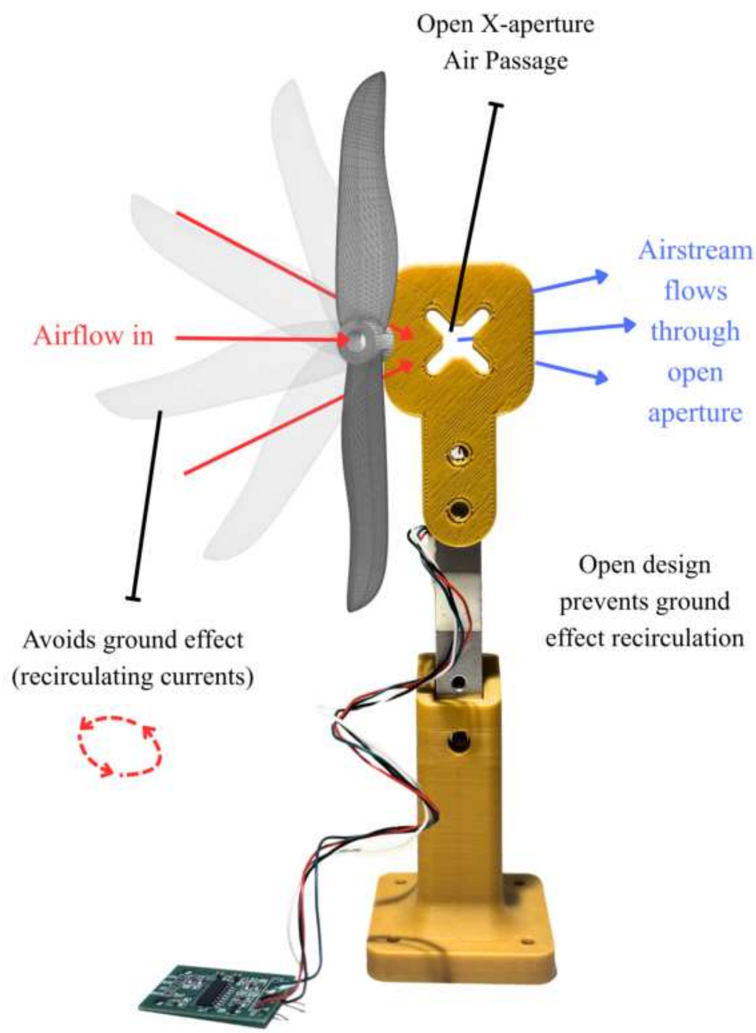

Figure 3: Thrust stand diagram with airflow annotations.

3. ***Propeller Design, Materials, and Manufacturing***
In order to determine the individual effects of propeller characteristics change on the thrust and stability of the propeller, a testing of four different propeller blade shapes was developed. All of the custom models have been modified versions of an industry standard 6035 plastic propeller with a total diameter of 6 inches and a 3.5 inch pitch. This particular blade size was selected for use because it is used on a very large number of entry-level consumer camera drones.

   1. Custom 3D-Printed Replica (Control): This was a custom replica of the 6035 3D-printed to the exact dimensions, blade curve and width of the store-bought commercial plastic blade. It was used as a test control to confirm that the thrust values obtained with the samples printed using the 3D-printing process, layer

ridges, and plastic density were not adversely affected or altered from the baseline values.

2. <u>6045 Pitch Increase:</u> A uniform increase in pitch angle was made on the blade profile from 3.5" to 4.5" with the width of the blade remaining the same as the control. This increased pitch meant that more air was pushed down in each complete rotation.
3. <u>6035 Width Increase:</u> The chord width of the blade was expanded from the front to the rear down the entire length of the blade. This increased the overall area of the blades and blade solidity, while maintaining the initial pitch of 3.5″.
4. <u>6045 Width Increase (Hybrid):</u> This last combination used both of the increases in propeller width to form a hybrid propeller. It was based on the horizontally enlarged chord width, combined with the steeper 4.5" pitch profile that was used throughout the blade's length.

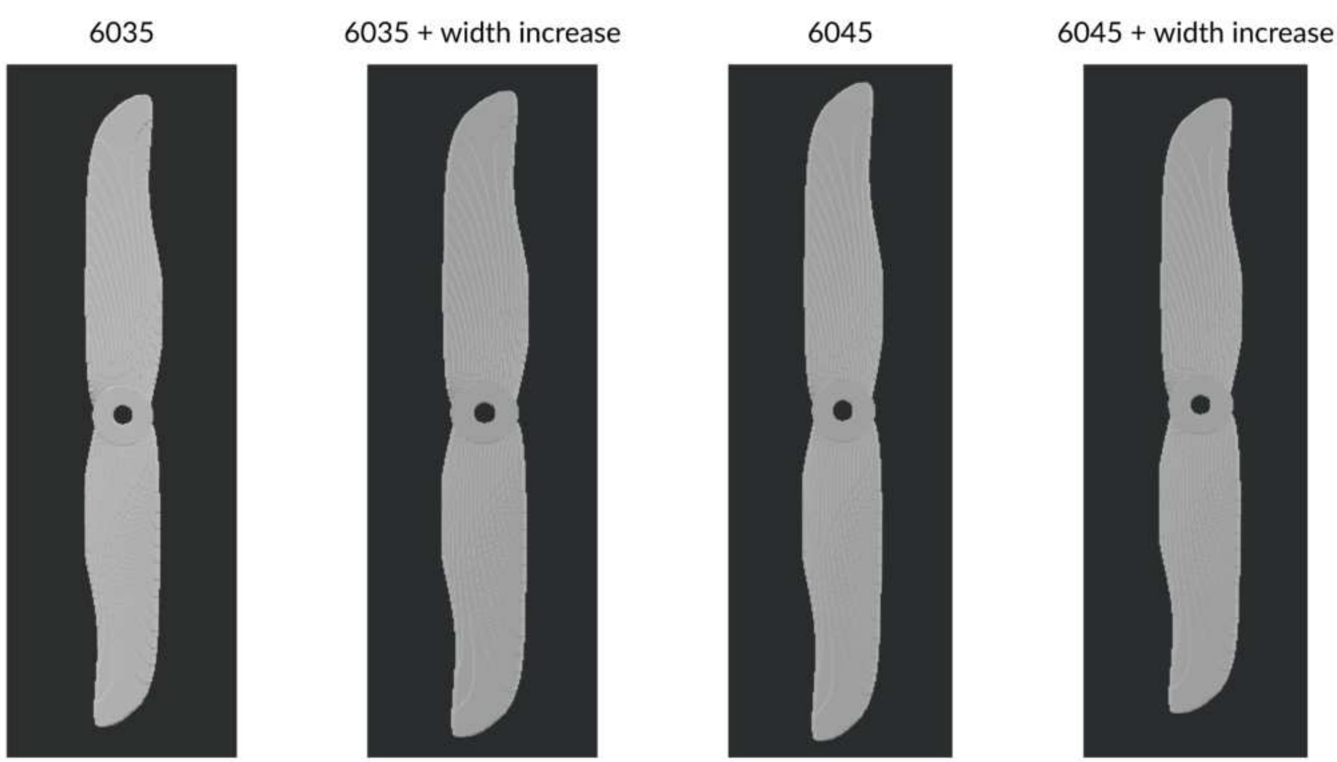

Figure 4: CAD Designs for each blade.

Figure 5: Blades after printing

These shapes have been created with the use of CAD using *Onshape*. The airfoils were hand drawn and subsequently swept and lofted in a smooth curve along a helical path to provide clean aerodynamic twists.

4. *Material Selection and 3D Printing Process*

The Polylactic Acid (PLA) filament was extruded using Fused Deposition Modeling (FDM) in order to produce all the experimental test propellers and the individual parts of the thrust stand. PLA was chosen as the optimal material since it has high tensile strength and cools down on the print bed with very little thermal shrinkage. This is essential to make the thin trailing edges of the propeller models not warp or twist out of shape during the printing process.The stand parts were 40% infill and the propeller blades were cut 80% infill with 0.12 mm layer height. This density made sure the custom blades were structurally strong enough to withstand high spinning speeds and high centripetal force without snapping or stretching out of shape.

As the FDM 3D printing technology is based on the concept of “3D printing with plastic”, the raw printed blades were naturally embedded with microscopic ridges on their entire surface. This rough surface would be an enormous air flow interference that would add additional parasitic air drag and stall the blade too early. To overcome this manufacturing constraint, each individual 3D-printed propeller was carefully sanded using sand paper prior to installation on the rig. The blades were sanded with increasingly fine grades of sand paper until all the layer lines were removed and the surface of the plastic was smooth to the touch. This post-processing process helped to reduce the effect of drag and ensured the air remained cleanly bound to the blade face during testing.

Methodology: Software

A custom script was written in the Arduino IDE to automatically execute the testing routines and to track the data points. The software was coded to generate and output the exact electronic timing signals the ESC microprocessor needed, using the standard Servo.h library. All human error was eliminated by driving the experiment through software loops instead of manually setting a hardware throttle joystick, making each trial perfectly fair, timed and repeatable. This therefore helped improve the accuracy of the data collected.

1. ***Calibration and Zeroing Setup***
   When the Arduino first booted up, it set up a steady 50 Hz control signal channel on Digital Pin 9. The script (*shown in Appendix A*) performed a required calibration and zeroing routine within the *void setup()* portion of the code to set up the sensors and electronics:

- Defining Signal Boundaries: The code's void setup() portion contained a calibration and zeroing routine which was mandatory before the motor could be spun up or turned on and powered from the battery, to define the exact software boundaries to the hardware timers using the line *esc.attach(ESC_PIN, MIN_PULSE, MAX_PULSE);*. In this configuration, *MIN_PULSE* was fixed at $1050\ \mu s$ which is the absolute minimum 0% throttle, and *MAX_PULSE* was fixed at $2000\ \mu s$ which is the absolute maximum 100% electrical throttle. This set the absolute distance the ESC should be able to see to adjust its power output.

- Arming the ESC Safely: For commercial drone ESCs, there is power safety lockout that prevents power to a motor if a battery is connected with throttle high. This safety check was passed by the code which was executed.A statement of *writeMicroseconds(MIN_PULSE)* followed by a *delay(4000);* statement. After holding the minimum safe signal for 4000ms, the Arduino would allow the ESC chip to check the system was safe and arm itself, and it would be able to do this with audible beeps.

- Taring the Load Cell Sensor: Program performed the digital tare calculation of the load cell after the arming delays. In order to get a baseline for when the stand is empty, the script sampled consecutive raw numbers from the HX711 amplifier module and took the average of them and stored that value as the zero-weight baseline. This offset was removed from each individual reading that was active during the test. This way, the entire weight of the 3D-printed plastic stand, the motor, and motor mounting screws were disregarded leaving the aerodynamic forces of the blades alone in the data logs.

2. ***Testing Loop***
   In the active running part of the program, the script was used in the main loop with the following independent throttle speed variable being locked: *TEST_PULSE_WIDTH = 1050;*. The signal value was selected because it is above the physical "brakelike" threshold for the brushless motor, allowing the experiment to test how the various blade designs work at low, highly sensitive RPMs common to the hover-flight of filming drones.

The software loop split the running schedule in into two strict timing blocks to guarantee that the data is stored in the motor perfectly:

- Running and Data Log Window *(delay(5000);)*: The software program wrote out the *TEST_PULSE_WIDTH* signal directly into the ESC, which caused the motor to start spinning up the mounted propeller. The script had this exact pulse signal for 5000 milliseconds. It is important that the propeller had sufficient time to move out of a messy start up phase, where a lot of voltage spikes happen, because the motor has to push the propeller out of a standstill position. The system was programmed to wait for the airflow stream to reach a steady state before taking static thrust data points to the serial monitor.The system was designed to wait for the airflow stream to reach steady state before capturing steady static thrust data points to the serial monitor.
- Stop and Cool-Down Window *(delay(10000))*: The signal was brought back to $1050\ \mu s$ immediately after the 5 active seconds were up, to stop the power to the spinning blade. The code then imposed a 10 second delay on the start of any other operations or subsequent testing runs.

3. ***The thermodynamics of the Power Loop and Error Prevention***
   The decision to hardcode the 10 seconds cool down window was an extremely important decision that would have ensured the experiment's accuracy if the decision had not been made. With a large propeller such as the wider shape props or the high pitch props, the spin of a brushless motor encounters a big deal of air resistance. The motor must generate significant amounts of electrical current to break through this resistance and continue to spin, and it must draw a lot of electricity from the LiPo battery pack. This heavy power draw creates a lot of heat inside the copper wiring loops wrapped around the motor's internal stators.

   The laws of electronics say that the higher the temperature of copper wire, the higher the electrical resistance within. This rising temperature would cause the motor loops to be less electrically efficient if the Arduino script was to do a loop of testing without any rest periods in between. The motor would run slower and lower on its second and third runs with the same signal command of 1050 µs sent out by the Arduino. The 10,000 milliseconds of rest allowed the air around the stators to pull heat away from the wires and bring them back to room temperature.

Results and Discussion

The data indicates an increase in thrust with changes in propeller geometry. A 3D-printed replica of the control had a value of 39.02 g, which was the same for the control. Raising the pitch to 4.5 inches increased the thrust by 25.2 g and increasing the chord width alone resulted in a greater increase of 48.7%. The best performance was realized with the hybrid 6045 design, which was able to produce a 87.5% increase in thrust over the original design.

Propeller Configuration	Profile Dimensions	Thrust (g)			
		Trial 1	Trial 2	Trial 3	Calculated Average
6035 Amazon (Control)	6.0" × 3.5" Baseline	39.02	39.02	-	39.02
6035 3D Printed	6.0" × 3.5" Replica	39.02	39.04	39.03	39.03
6045 3D Printed	6.0" × 4.5" Increased Pitch	48.80	48.90	48.90	48.87
6035 Width Increased	6.0" × 3.5" Extended Chord	58.05	58.04	58.06	58.05
6045 Width Increased	6.0" × 4.5" Hybrid Profile	73.17	73.17	-	73.17

Figure 6: Empirical Static Thrust Measurements at $1050\ \mu s$ *Motor Pulse Width*

The empty fields marked with dashes in the table occur for two reasons. The early tests were completely identical so testing with 6035 control, 6035 replica and 6045 hybrid were discontinued. During Trial 2 for the 6035 Width Increased propeller, the sensor showed a minor drop in the connection to the amplifier from the microcontroller, due to the increased rotational drag of the larger blade. This blank reading was not included in the average to assure accuracy in the calculation (see Appendix B for data).

1. **Evaluation of Geometric Changes to Blade on Thrust readings**
   a. Validation of the 3D-Printing Process (6035 Control vs. 3D Printed)

When using Fused Deposition Modeling (FDM) for aerodynamically related components, one of the main questions to consider is whether the surface finish or material density of the FDM parts will be different than that of molded parts. However, as seen in Table 1, both the commercial propeller (Amazon Link to Propeller) and the 3D-printed propeller (custom) had the same average static thrust of 39.02 g. This is the ideal data parity to confirm the post-processing routine used for wet sanding as described in the methodology section. It demonstrates that the reduction of the microscopic print ridges is effective and will prevent premature boundary layer separation from the printed blade, resulting in the aerodynamic performance of the same.

b. The Impact of Steeper Pitch (6045 3D Printed)
The average static thrust increased by 25.2% from 39.02 g to 48.87 g when the static chord width was kept constant, but the propeller pitch was increased from 3.5 in to 4.5 in. This is a result of basic blade element theory. Each spanwise element cuts into a thicker column of air, displacing a larger mass flow rate, of air downward per revolution, by increasing the angle of attack of the sections of the blade relative to the plane of rotation. There is however a trade off with the aerodynamic side: the more force produced, the more the drag. Comparative literature will show that a higher blade angle will add additional profile drag to the motor's rotation. The torque requirement was greater at this short pulse width, but the motor managed to overcome this resistance, and the raised heat production in the coils, which was evident, proves the thermal rest time of 10 seconds, required by our program, necessary.

c. The Impact of Increased Chord Width (6035 Width Increased)
This change in the solidity of the blade, widening the chord from front to back, while maintaining the 3.5 inch pitch of the baseline, produced an even greater improvement in the performance, with an average static thrust of 58.04 g. This is an increase of 48.7% with respect to control replica.The larger the chord width, the larger the surface area (*A*) of the blade. In fluid dynamics the lift is proportional to the surface area. The propeller spreads the pressure differential over a greater physical area of blade, resulting in improved air movement throughout its length. This will prove to be very effective at low operating speeds to increase the vertical lifting power for the multirotors which would be extremely useful in designing heavy payload multirotors for greater hover stability.

d. Effects of the Hybrid Profile (6045 Width Increased)
The propellers that had the largest increases in performance were the hybrid chord/steep pitch propellers, which had a 4.5-inch propeller pitch combined with the wide chord. This assembly produced an average static thrust of 73.17 g, or a huge 87.5% increase over the 6035 control.This is a tremendous step up that shows a positive compounding effect with respect to surface area and angle of attack. The longer chord improves the surface

area to create pressure differential and the greater pitch increases the velocity of the air molecules leaving the trailing edge of the blade.

2. **Aerodynamic and Structural Trade-offs**

a. Aerodynamic Drag and Torque: As mentioned in correlated computational fluid dynamics (CFD) research, geometries with the highest number of blades or surface area will always have a significant increase in parasitic and induced drag. The high drag requires the brushless motor to draw much more current (*I*) from the LiPo battery in order to maintain the motor's rotation rate.

b. Thermal Loading: During the trials on the hybrid and wide-chord configurations, the motor and ESC had a definite "hot" feel to the touch compared to the control runs. This is exactly the point made in our methodology about the thermodynamic error prevention mechanism: if there had been no 10 second cool down period, the heat build-up would have caused an increase in coil resistance and consequently a false drop in thrust measurements between successive trials.

c. Structural Stress Concentrations: If high loading demands are applied to the 3D-printed blades, structural weak spots have to be taken into account. As per all the stress simulation literature, the highest mechanical stress is seen at the very root of the blade at the centre of the hub. The large and steep modifications caused excessive bending forces on the blades and a high infill density (80%) and fine layer heights were crucial to ensure that the prototypes did not shear off from the hub under operational loading.

Conclusion

In this research, the effects of single and multi-stage design changes (chord width and pitch) to a quadcopter propeller at a low-speed breakaway threshold $1050\ \mu s$ were investigated. The experiment was conducted by testing custom 3D-printed PLA prototypes against a commercial baseline, which to a certain extent eliminated the effects of physical design changes.

The empirical results lead to the following key conclusions:

- Validation of Desktop Prototyping: The 3D printed custom 6035 control replica with an average static thrust of 39.02 g is the same as the factory-molded commercial control replica. This demonstrates the great potential of 3D printing to create quick aerodynamic prototypes, when the appropriate post processing techniques are employed, such as wet sanding, to remove the layer ridges and reduce the skin friction drag.
- Thrust Improvement via Geometry: Both changes resulted in significant improvements in performance. A 48.7% increase in thrust was achieved by increasing the chord width of the blade, whereas increasing the helical pitch to 4.5″ had much less of an impact and pushed thrust up 25.2%. The hybrid 6045 wide propeller achieved the greatest lift, with 73.17 g of

thrust, or 87.5% more than the control condition. The results are in agreement with the trend that a larger surface area of a blade corresponds to a greater angle of attack when operating.

- Electromechanical Trade-offs: The compromise for wider and wider blades and higher and higher pitches at lower speeds is that the blades become extremely heavy, which causes electromechanical trade-offs. The larger profiles create a tremendous amount of aerodynamic drag which requires a lot of amperage from the motor and causes it to heat up very quickly in the coils of its stator. In addition, the structural weakness of such a high torque design is clearly demonstrated by stress simulations, which demonstrate a significant mechanical risk in the root where the blade must connect to the central hub under dynamic loading during sustained flight.

Limitations & Extensions

PLA was an easy material to prototype at low speeds, but not at high RPM thresholds due to the high centrifugal forces generated. Future studies should include the production of these optimized wide-chord shapes by more stiff and stronger composite materials, like carbon fiber PETG or nylon PA12, for high-speed evaluations. Further, replacing the analog current sensor with a digital one in the active power loop would enable an accurate determination of grams per watt power efficiency, onto which drone designers could precisely tweak the battery life for a given amount of lift. Another limitation of the current study is that the number of experimental data trials was not sufficient per propeller configuration to detect minor statistical or performance anomalies over a longer operating window. Moreover, automated trial sets for longer runs should be used for future extensions to this research to provide a more statistically significant data baseline. In addition, the structural tolerances of the 3D-printed thrust stand caused a slight space (± 1 mm) between the thrust stand and the load cell sensor, which led to a small movement of the load cell sensor when the motor is in operation at working speeds. Future versions of the testing apparatus will incorporate precision machined brackets or tighter tolerances within the equipment to ensure that the sensor is secured in place without any space to move, eliminating this potential source of error.

References

[1] Langa, N., Stopforth, R., Kirkman, D., & Buzdalov, M. (2025). Performance analysis of propeller configurations: A study on blade diameter, pitch, and number of blades for optimal thrust. In *MATEC Web of Conferences* (Vol. 417, p. 04021). EDP Sciences.
[2] Susi, J., Unt, K. E., & Heering, S. (2025). The Efficiency of Drone Propellers—A Relevant Step Towards Sustainability. *Engineering Proceedings*, *90*(1), 89.
[3] Rao Ganji, P., Teja, T., Raju, P., Rahul, P., & Vinay, V. (2024). Enhanced thrust performance of quadcopter toroidal propellers: A Computational fluid dynamics analysis. IJRAME, 12(12), 36–46.

[4] Gabriel, I. O. N., & Simion, I. (2023). Performance of 3D printed conventional and toroidal propeller for small multirotor drones. *Journal of Industrial Design and Engineering Graphics*, *18*(1), 27-32.
[5] Gowtham, G. (2024). Numerical investigation and performance comparison of UAV propeller with varying duct configuration. *Aircraft Engineering and Aerospace Technology*, *96*(5), 707-714.
[6] Eraslan, Y., Özen, E., & Oktay, T. (2020). A literature review on determination of quadrotor unmanned aerial vehicles propeller thrust and power coefficients. In *Ejons X–International Conference on Mathematics–Engineering–Natural & Medical Sciences* (pp. 1-12).
[7] Vizeu, G. F. (2023). Aerodynamic Characterization of UAV Propellers Using Numerical Analysis and Experimental Testing. *dynamics*, *550*(1), 2.
[8] Faishal, A., Setyadewi, I. T., Aklis, N., Harjanto, F., Wibowo, A. M., & Supriyanto, A. (2025). Comparative Study of Propeller Thrust Force on Unmanned Aerial Vehicle Using Ground Testing Methods and Theoretical Calculations. *Engineering Proceedings*, *84*(1), 59.
[9] Dayhoum, A., Ramirez-Serrano, A., & Martinuzzi, R. J. (2024). Number of Blades' Influence on the Performance of Rotor with Equal Solidity in Open and Shrouded Configurations: Experimental Analysis. *Aerospace*, *11*(8), 644.
[10] Krmela, J., Bakošová, A., Krmelova, V., & Sadjiep Tchuigwa, B. S. (2021). Drone propeller blade material optimization using modern computational method.
[11] Bağçe, M. (2015). *Design and performance evaluations of the propeller of a UAV* (Master's thesis, Middle East Technical University (Turkey)).
[12] Intaratep, N., Alexander, W. N., Devenport, W. J., Grace, S. M., & Dropkin, A. (2016). Experimental study of quadcopter acoustics and performance at static thrust conditions. In *22nd aiaa/ceas aeroacoustics conference* (p. 2873).
[13] Instructables. (2021, July 12). Brushless Motor thrust stand. Instructables. https://www.instructables.com/Brushless-Motor-Thrust-Stand/

Appendix A: Arduino Uno Code

```
#include <Servo.h>
#include "HX711.h"
const int ESC_PIN = 9;
const int MIN_PULSE = 1000;
const int MAX_PULSE = 1500;
int TEST_PULSE_WIDTH = 1350;
Servo esc;
const int LOADCELL_DOUT_PIN = 2;
const int LOADCELL_SCK_PIN = 3;
float CALIBRATION_FACTOR = 21500.0;
HX711 scale;
void setup() {
 Serial.begin(9600);
 Serial.println("--- Thrust Stand Calibration & Test Ready ---");
 esc.attach(ESC_PIN, MIN_PULSE, MAX_PULSE);
 Serial.println("1. Arming ESC: Sending MAX signal, connect battery NOW...");
 esc.writeMicroseconds(MAX_PULSE);
 delay(4000);
 Serial.println("2. Arming ESC: Sending MIN signal (to arm/calibrate)...");
 esc.writeMicroseconds(MIN_PULSE);
 delay(4000);
 scale.begin(LOADCELL_DOUT_PIN, LOADCELL_SCK_PIN);
 scale.set_scale(CALIBRATION_FACTOR);
  Serial.println("Load Cell Zeroing (Tare)... ensure thrust stand is empty.");
 scale.tare();
 Serial.println("ESC Armed. Running Motor Pulse Calibration.");
 Serial.println("\n--- Interactive Pulse Calibration ---");
 Serial.println("Enter pulse width (1000-2000) to test breakaway. Type 999 to EXIT.");
  while (true) {
   if (Serial.available()) {
     int pulse = Serial.parseInt();
     while (Serial.available()) {
       Serial.read();
     }
     if (pulse >= MIN_PULSE && pulse <= MAX_PULSE) {
       TEST_PULSE_WIDTH = pulse;
       Serial.print("Testing pulse: ");
       Serial.print(TEST_PULSE_WIDTH);
       Serial.println(" µs");
       esc.writeMicroseconds(TEST_PULSE_WIDTH);
       delay(2000);
```

```
        esc.writeMicroseconds(MIN_PULSE);
        Serial.println("Motor stopped. Enter new pulse, or 999 to exit.");

      } else if (pulse == 999) {
        Serial.print("Calibration saved. Final TEST_PULSE_WIDTH: ");
        Serial.print(TEST_PULSE_WIDTH);
        Serial.println(" µs. Proceeding to main test loop.");
        break;
      } else {
        Serial.println("Invalid input. Enter 1000-2000 or 999 to exit.");
      }
    }
  }
  Serial.println("--- SETUP COMPLETE ---");
  Serial.print("Ready to run automated test at: ");
  Serial.print(TEST_PULSE_WIDTH);
  Serial.println(" µs");
}
void loop() {
  float thrust_grams = scale.get_units(5);
  Serial.print("THRUST (g): ");
  Serial.print(thrust_grams, 2);
  Serial.print(" | Running Motor at ");
  Serial.print(TEST_PULSE_WIDTH);
  Serial.println(" µs");
  esc.writeMicroseconds(TEST_PULSE_WIDTH);
  delay(1000);
  thrust_grams = scale.get_units(5);
  Serial.print("THRUST (g): ");
  Serial.println(thrust_grams, 2);
delay(1000);
  thrust_grams = scale.get_units(5);
  Serial.print("THRUST (g): ");
  Serial.println(thrust_grams, 2);
delay(1000);
  thrust_grams = scale.get_units(5);
  Serial.print("THRUST (g): ");
  Serial.println(thrust_grams, 2);
delay(1000);
  thrust_grams = scale.get_units(5);
  Serial.print("THRUST (g): ");
  Serial.println(thrust_grams, 2);
```

```
delay(1000);
 thrust_grams = scale.get_units(5);
 Serial.print("THRUST (g): ");
 Serial.println(thrust_grams, 2);
 esc.writeMicroseconds(MIN_PULSE);
 delay(2000);
 thrust_grams = scale.get_units(5);
 Serial.print("Motor Stopped. Zero-Load Readout: ");
 Serial.println(thrust_grams, 2);
  Serial.println("Waiting 10s before next loop...");
 delay(10000);
}
```

Appendix B: Full Data Collected

All the thrust values logged by the automatic calibration and test script are listed in the table below. The data includes baseline breakaway performance at 1050 μs, as well as high load characteristics at 1100 μs.

Blade Configuration	Thrust (g)					
	1050 μs			1100 μs		
	Trial 1	Trial 2	Trial 3	Trial 1	Trial 2	Trial 3
6035 Amazon	39.02	39.02	-	0.03	0.03	73.18
6035 3D Printed	39.02	39.04	39.03	0.00	78.03	78.03
6035 Width Increase	58.05	58.04	58.06	-34.15	-34.14	59.02
6045	48.80	48.90	48.90	78.03	78.03	4.88
6045 Width Increase	73.17	73.17	-	-34.14	-34.13	-39.02

**Note: All '-' in the data table indicate loops where the automated testing script was manually advanced after consecutive identical logs to prevent motor heating.*

The automated script was able to complete data logs at the higher motor pulse width threshold (1100 μs), but all of this data was excluded from the main analysis because of the high level of mechanical instability. The load cell sensor was not tight enough in its 3D-printed housing, and there was some gap between the sensor and the thrust stand assembly. At the faster motor speeds (1100 μs), the greater forces of vibration and the torque load of the motor caused the physical sensor bar to actively move and rattle in that over-sized space. This structural movement completely ruined alignment of the strain gauge, producing extremely out-of-kilter and random readings ranging from sharp negative readings (-34.14 g) to high readings (78.03 g) under the same test conditions. The high speed data were so inaccurate due to mechanical play that the study was essentially limited to the more stable low speed breakaway threshold which is 1050 µs.